

Total 3D imaging of phase objects using defocusing microscopy: application to red blood cells

P. M. S. Roma¹, L. Siman¹, F. T. Amaral², U. Agero¹ and O. N. Mesquita^{1, a)}

¹*Departamento de Física, ²Programa de Pós Graduação em Engenharia Elétrica, Universidade Federal de Minas Gerais, Caixa Postal 702, CEP 31270-901, Belo Horizonte, MG, Brazil.*

We present Defocusing Microscopy (DM), a bright-field optical microscopy technique able to perform total 3D imaging of transparent objects. By total 3D imaging we mean the determination of the actual shapes of the upper and lower surfaces of a phase object. We propose a new methodology using DM and apply it to red blood cells subject to different osmolality conditions: hypotonic, isotonic and hypertonic solutions. For each situation the shape of the upper and lower cell surface-membranes (lipid bilayer/cytoskeleton) are completely recovered, displaying the deformation of RBCs surfaces due to adhesion on the glass-substrate. The axial resolution of our technique allowed us to image surface-membranes separated by distances as small as 300 nm. Finally, we determine volume, superficial area, sphericity index and RBCs refractive index for each osmotic condition.

Standard optical microscopy imaging of phase objects is generally obtained with microscopes operating in Phase Contrast or Nomarsky configurations^{1,2}. However, even for objects with uniform refractive index these techniques present difficulties for obtaining accurate full-field thickness profiles. Recently, new approaches known as quantitative phase microscopy techniques³⁻⁷, have adequately obtained full-field height profile of phase objects with successful application in living cells. Despite that, in the case of red blood cells (RBCs) these techniques are only able to provide the thickness profile and thickness amplitude fluctuations, such that height profile information of each particular cell surface-membrane (lipid bilayer/cytoskeleton) is not accessed.

Using Defocusing Microscopy (DM), we present a new method able to perform total 3D imaging of RBC, and thus, capable of determining the actual shape of the cell's upper and lower surface-membranes, separately. New procedures to retrieve RBC volume, superficial area, sphericity index and refractive index using DM are also exposed. All developed methods are applied to data of 25 RBCs immersed in three different solutions: hypotonic (200 mOsm/kg), isotonic (300 mOsm/kg) and hypertonic (400 mOsm/kg), showing the differences in the lower membrane adhesion to the glass substrate. For assessment of bio-mechanical properties along the RBCs surfaces, nanometer height fluctuations for each interface can be obtained separately, such that the effect of adhesion to the substrate can also be evaluated^{8,9}. A defocusing technique has been recently applied for 3D imaging of cells using a phase contrast microscope under white-light illumination, with transverse resolution of 350 nm and axial resolution of 900 nm¹⁰. This technique cannot resolve surface-membranes separated by an axial distance smaller than 900 nm, which is the case of most RBCs. Strikingly, our Defocusing Microscopy technique, using a bright-field defocused microscope and our

theoretical framework, can resolve surface-membranes of RBCs separated by axial distances down to 300 nm.

Transparent objects that would be invisible in a standard bright-field optical microscope can turn visible by defocusing the microscope, since the act of defocusing introduces a phase difference between the diffracted orders and the non-diffracted transmitted order (zero order). From contrast intensity measurements of images in two focal positions, one can obtain information about the phase of the optical electric field and reconstruct the height profile of the phase object. The formalism of Intensity Equation has been used for this purpose^{3,11}, but in its present form there are no explicit phase terms taking into account the distance between the objective focal plane and the diffracting surfaces, such that the total 3D imaging is not feasible. In our approach, Fresnel Diffraction Theory and the formalism of propagation of the Angular Spectrum^{12,13} are used in order to propagate the light electric field throughout our defocused microscope. We treat the electric field as a scalar quantity and neglect polarization effects. As a result, the defocused electric field is represented by an integral over the diffracted wave-vectors (\vec{q}), where the positions of the objective focal plane (z_f) and the phase object surfaces appear explicitly, allowing us to obtain total 3D imaging of phase objects. Our model works for pure phase objects, such that in the case of RBCs the illumination light should be red filtered to minimize light absorption. For the total 3D imaging using DM, coherence of the illumination light is not an important issue. More details of the experimental set up are given in the supplementary material¹⁴.

In the model presented, all parameters associated to optical elements that are displaced to produce image defocusing are known⁹. In our derivation below, defocusing is caused by the displacement of the microscope objective, which can be related to the displacement of other elements, as will be shown later. The results obtained are independent of the origin of the reference frame along z , adopted here as the plane where the RBC contrast has a minimum value, that corresponds to cell largest diameter plane. The defocused light electric field that

^{a)}E-mail me at: mesquita@fisica.ufmg.br

passes through a red blood cell (Fig.1a) can be written as^{8,9,15-18},

$$E(\vec{\rho}, z_f) = \frac{1}{(2\pi)^2} \int_{-\infty}^{+\infty} [A_1(\vec{q}) e^{i\vec{q}\cdot\vec{\rho}} e^{i(\frac{z_f - h_1(\vec{\rho})}{2k})q^2} + A_2(\vec{q}) e^{i\vec{q}\cdot\vec{\rho}} e^{i(\frac{z_f - h_2(\vec{\rho})}{2k})q^2}] d\vec{q}, \quad (1)$$

where $h_1(\vec{\rho})$, $h_2(\vec{\rho})$ are the coordinates for the upper and lower RBC surface-membranes, respectively, $k = n_{ob}k_0$ is the light wavenumber, with n_{ob} the objective immersion medium index of refraction and k_0 the wavenumber in vacuum. The terms

$$A_1(\vec{q}) = \int_{-\infty}^{+\infty} E_0 e^{-i\vec{q}\cdot\vec{\rho}} e^{i\Delta n k_0 h_1(\vec{\rho})} d\vec{\rho}$$

$$A_2(\vec{q}) = \int_{-\infty}^{+\infty} E_0 e^{-i\vec{q}\cdot\vec{\rho}} e^{-i\Delta n k_0 h_2(\vec{\rho})} d\vec{\rho} \quad (2)$$

are the Angular Spectra of the electric field diffracted by the surface-membranes. Additionally, Δn is the refractive index difference between the RBC and its surrounding medium (uniform inside the RBC), and $h_{1/2}(\vec{\rho}, t) = h_{1/2}(\vec{\rho}) + u(\vec{\rho}, t)$, such that the time average $\langle h_{1/2}(\vec{\rho}, t) \rangle = h_{1/2}(\vec{\rho})$ and $u(\vec{\rho}, t)$ is the out-of-plane height fluctuations in the nanometer range. Since we are interested in equilibrium shapes of RBCs, Eqs. (1) and (2) are time averaged quantities. The second order cross terms $A_1(\vec{q}) \cdot A_2(\vec{q})$ are neglected (in the worst case $(\Delta n k_0)^2 h_1 h_2 < 1$), which means that the incident light is diffracted by only one interface and the chance of being diffracted by the two interfaces is small. Naturally, higher order terms can be included into the model if they become necessary for a better quality 3D image.

Defining the image contrast as $C(\vec{\rho}) = \frac{I(\vec{\rho}) - I_0}{I_0}$, where $I(\vec{\rho})$ is the intensity of the object image and I_0 is the background intensity, for first-order diffraction, the DM contrast for a red cell decomposed in spatial Fourier components \vec{q} is,

$$C(\vec{\rho}) = \frac{2\Delta n k_0}{\sqrt{A}} \left\{ \sum_{\vec{q}} \left[h_2(\vec{q}) \sin\left(\frac{(z_f - h_2(\vec{\rho}))q^2}{2k}\right) - h_1(\vec{q}) \sin\left(\frac{(z_f - h_1(\vec{\rho}))q^2}{2k}\right) \right] \sin(\vec{q}\cdot\vec{\rho}) \right\}, \quad (3)$$

where A is the RBC surface area and $h(\vec{\rho}) = \frac{1}{\sqrt{A}} \sum_{\vec{q}} h(\vec{q}) \sin(\vec{q}\cdot\vec{\rho})$. For the chosen reference frame, $h_1(\vec{\rho}) > 0$ and $h_2(\vec{\rho}) < 0$, but for convenience we will use positive quantities, such that $h_2 = -|h_2|$. For small defocusing distances the approximation $\sin((z_f - h)q^2/2n_{ob}k_0) \simeq (z_f - h)q^2/2n_{ob}k_0$ can be used, resulting in the DM contrast,

$$C(\vec{\rho}) = \frac{\Delta n}{n_{ob}} \left[\left(z_f - h_1(\vec{\rho}) \right) \nabla^2 h_1(\vec{\rho}) + \left(z_f + |h_2(\vec{\rho})| \right) \nabla^2 |h_2(\vec{\rho})| \right], \quad (4)$$

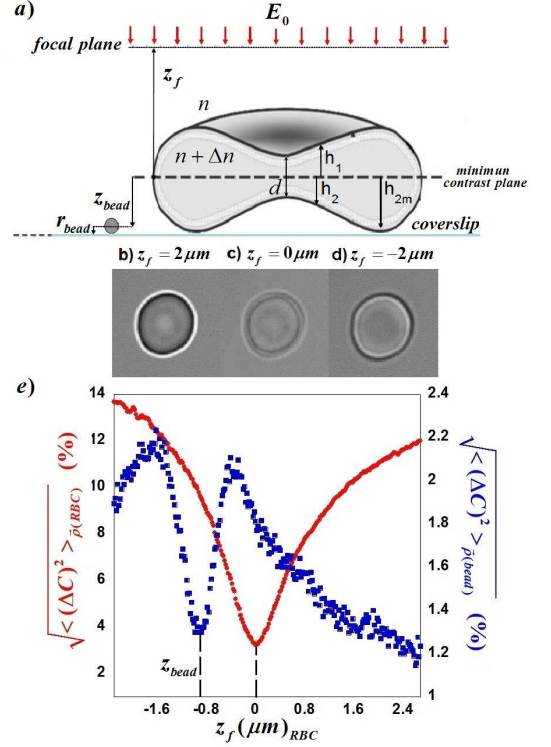


FIG. 1. (a) RBC model with the reference frame origin at the cell minimum contrast plane, defining $h_1 > 0$ and $h_2 < 0$ as the coordinates of the upper and lower surface-membranes, respectively. (b-d) Contrast images of a RBC at different defocusing distances z_f . (e) Contrast standard deviation profile as a function of defocusing distance z_f for a RBC and the bead. The minimum values for both profiles are clearly determined, and the distance between them is $|z_{bead}|$, such that $|h_{2m}| = |z_{bead}| + |r_{bead}| = |z_{bead}| + 0.099\mu m$.

with $\frac{1}{\sqrt{A}} \sum_{\vec{q}} h(\vec{q}) \sin(\vec{q}\cdot\vec{\rho}) q^2 = -\nabla^2 h(\vec{\rho})$. From this expression we note that DM contrast is proportional to the object's local curvature ($\nabla^2 h \equiv \kappa$). Therefore, the flat glass-substrate is not visualized with DM. The limit of validity of Eq. (4) can be checked by measuring the linear region of $C \times z_f$. For RBC this limit is $z = \pm 2\mu m$ in relation to the middle plane (minimum contrast plane). Since the roughness of the interface $u(\vec{\rho}, t)$ can have large spatial wavenumbers q , Eq. (3) must be used to analyze height fluctuations of the RBC surface-membranes^{8,9}.

It is important to stress that the introduction of the surface-membranes height coordinates, $h_1(\vec{\rho})$ and $h_2(\vec{\rho})$, into the phase factors $((z_f - h_{1/2})q^2/2k)$ in Eq. (1), that allowed us to achieve total 3D imaging. None of the previous approaches using defocusing techniques had considered these important factors before. The coupling between $h(\vec{\rho})$ and $\nabla^2 h(\vec{\rho})$, as shown in Eq. (4), is responsible for the high axial resolution achieved by Defocusing Microscopy, as will be shown later.

To obtain RBC thickness profile and volume, one needs to measure the time-average cell contrast at two different

defocus distance: $\langle C_1 \rangle$ (at z_{f_1}) and $\langle C_2 \rangle$ (at z_{f_2}). Subtracting, pixel by pixel, the contrast image $\langle C_2 \rangle$ from $\langle C_1 \rangle$,

$$\langle C_2 \rangle - \langle C_1 \rangle = \frac{\Delta n}{n_{ob}}(z_{f_2} - z_{f_1}) \nabla^2 H, \quad (5)$$

where $H(\vec{\rho}) = h_1(\vec{\rho}) + |h_2(\vec{\rho})|$ is the cell thickness. Performing a Fourier transform on Eq. 5, the laplacian term gives rise to a $(-q^2)(h_1(\vec{q}) + |h_2(\vec{q})|)$ term, which divided by $-q^2$ and performing an inverse Fourier Transform,

$$H = \frac{n_{ob}}{\Delta n(z_{f_1} - z_{f_2})} \mathcal{F}^{-1} \left(\frac{\mathcal{F}\{\langle C_2 \rangle - \langle C_1 \rangle\}}{-q^2} \right). \quad (6)$$

If the values for z_f , n_{ob} and Δn are known, the thickness profile map of the observed cell is obtained. In addition, if the pixel area value is known, the cell volume $V = A_{pixel} \times H(\vec{\rho})$ is calculated. The mean thickness profiles for the 25 analyzed cells in hypotonic, isotonic, and hypertonic media are shown in the supplemental material¹⁴, and the mean volume values are shown in Table 1 and are in accordance with those reported by others techniques^{5,19,21,22}.

Using the thickness profile $H(\vec{\rho})$ and defining $\delta(\vec{\rho}) = h_1 - |h_2|$ as the asymmetry between the RBC surface-membranes h_1 and h_2 , we then have,

$$h_1(\vec{\rho}) = \frac{H(\vec{\rho}) + \delta(\vec{\rho})}{2} \quad h_2(\vec{\rho}) = \frac{-H(\vec{\rho}) + \delta(\vec{\rho})}{2}. \quad (7)$$

For $z_f = 0$, Eq. (4) can be rewritten as,

$$\nabla^2 \delta + \frac{\nabla^2 H}{H} \delta = -\frac{2n_{ob}}{\Delta n H} C(0, \vec{\rho}), \quad (8)$$

which is a non-homogeneous Helmholtz equation with variable coefficients, that can be numerically solved for $\delta(\vec{\rho})$ with the initial condition $\delta(\vec{\rho}) = 0$. Since $\frac{\nabla^2 H(\vec{\rho})}{H(\vec{\rho})}$ is a well-behaved function, the convergence of the fitting procedure is very robust. From the returned $\delta(\vec{\rho})$ the total 3D imaging is obtained, as shown in Fig.2 (a-f) (see also movies *S1 - S3* in supplementary materials¹⁴). The two extreme experimental points in the border of each interface are smoothly connected by a circumference, because diffraction at the border distorts the actual profile.

In Fig.2 (g-i), the average angular profiles for each group of RBCs subject to different osmotic pressures are displayed and the differences between the upper and lower membranes are evidenced. For hypotonic solution (Fig.2g), the upper membrane is inflated due to water entrance and the lower membrane remains attached to the glass-substrate. In the isotonic case (Fig.2h), it is seen that due to cell adhesion the lower membrane has a flatter height profile than the upper membrane, and for the hypertonic case (Fig.2i), the separation distance between the lower and the upper membrane decreases, and the

RBC exhibits a more pronounced dimple in the center region for both membranes. For all cases the adhesion contact region between the lower membrane and the glass-substrate is located (Fig.2b and c): isotonic $\rho = 2.5\mu\text{m}$ and hypertonic $\rho = 3\mu\text{m}$. Since the height profile and the pixel area are known, the cell surface area can be calcu-

late as $A = \int \sqrt{1 + \left(\frac{\partial h_{1/2}}{\partial x}\right)^2 + \left(\frac{\partial h_{1/2}}{\partial y}\right)^2} dx dy$. From the surface area and volume, we calculate the sphericity index $(\chi)^{23}$. All values are shown in Table 1 and are in accordance with those reported by other techniques^{21,24}.

The DM 3D imaging method is independent of the chosen reference system, and thus, it can be efficiently used to image red blood cells which are flowing through a glass capillary or a micro-fluidic device. To avoid moving the objective, one can use a beam-splitter to split the images and use two cameras focused in different positions to collect them. The relation between objective defocusing (Z_o) and camera defocusing (Z_c) is $Z_c = M^2 Z_o$, where M is the magnification of the objective. For a $M = 100X$ objective, the defocusing effect of a displacement of $1\mu\text{m}$ is obtained by displacing the camera by 1cm . Therefore, by using two cameras with an optical path difference of 1cm , the images recorded by each camera will correspond to the contrasts C_1 and C_2 of Eq. (5), where $z_{f_1} - z_{f_2} = 1\mu\text{m}$. The DM technique can also be used for total 3D imaging of high motility cells and to obtain information about the upper and lower membranes, the last one in dynamical contact with the substrate.

Defocusing Microscopy axial resolution depends on the sensitivity of image contrast measurement, optical contrast of the phase object, and mean curvature of the surfaces considered. For example, using our Eq. (4) at $\rho = 0$ and $z_f = h_1$, we obtain,

$$C(0, h_1) = \frac{\Delta n}{n_{ob}}(h_1 + |h_2|)\nabla^2 h_1, \quad (9)$$

and for $z_f = -|h_2|$,

$$C(0, h_2) = \frac{\Delta n}{n_{ob}}(-h_1 - |h_2|)\nabla^2 h_2, \quad (10)$$

such that $\Delta C = C(0, h_1) - C(0, h_2)$ then,

$$\Delta C = \frac{\Delta n}{n_{ob}}(h_1 + |h_2|)(\nabla^2 h_1 + \nabla^2 h_2). \quad (11)$$

For $\rho = 0$, $d = h_1 + |h_2|$ is the axial distance between the two surface-membranes in the RBC center, as shown in Fig. 1a, and since for RBCs

$$\nabla^2 h_1 \simeq \nabla^2 h_2 = \kappa, \quad (12)$$

where κ is the curvature of the surfaces then,

$$\Delta C = \frac{2\Delta n}{n_{ob}} d \kappa. \quad (13)$$

The minimum axial distance d_{min} is thus given by,

$$d_{min} = \frac{n_{ob}\Delta C_{min}}{2\Delta n\kappa}. \quad (14)$$

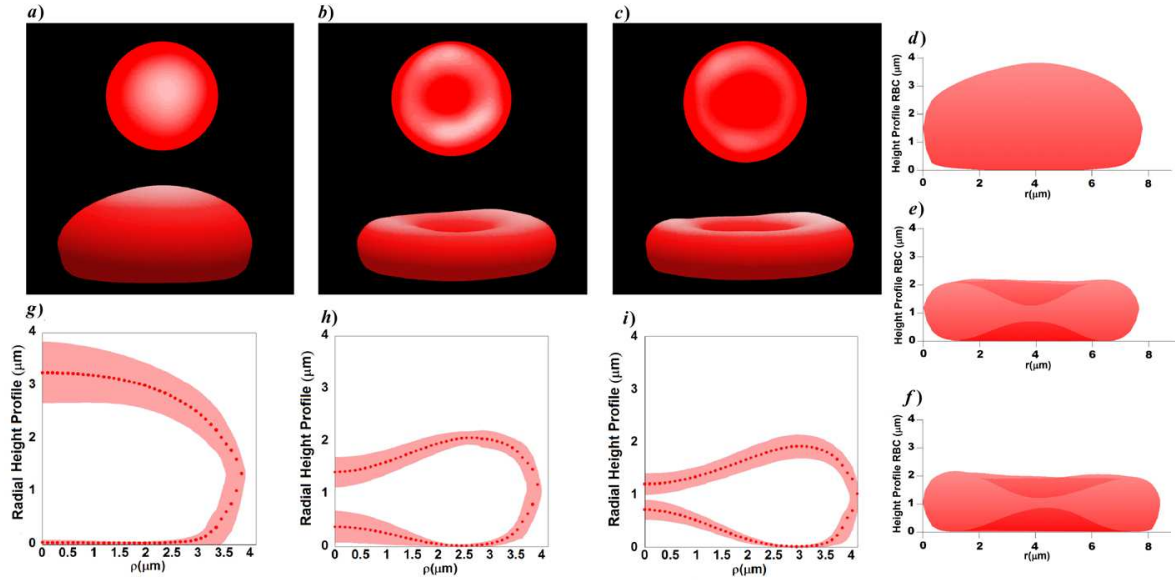


FIG. 2. Total 3D Imaging of red blood cells in (a/d) hypotonic (200 mOsm/Kg), (b/e) isotonic (300 mOsm/Kg) and (c/f) hypertonic (400 mOsm/Kg) solutions (Multimedia view). (g-i) Radial height profiles over all analyzed cells. The shaded areas represent the standard deviations of the average over the 25 RBCs.

TABLE I. Data on RBC osmolality, volume, surface area, sphericity index and RBC refractive index obtained from the full 3D imaging.

Osmolality (mOsm/Kg)	Radius(\bar{R}_M) (μm)	Volume (\bar{V}_M) (μm^3)	Surface Area(\bar{A}_M) (μm^2)	$\bar{\chi}$ --	n_{rbc} $\lambda = 610\text{nm}$
200 \pm 2	3.85 \pm 0.23	129 \pm 15	134 \pm 11	0.92 \pm 0.02	1.378 \pm 0.003
300 \pm 2	3.92 \pm 0.17	94 \pm 8	130 \pm 9	0.77 \pm 0.01	1.391 \pm 0.003
400 \pm 2	4.12 \pm 0.20	91 \pm 8	139 \pm 11	0.70 \pm 0.01	1.400 \pm 0.005

Using $\Delta C_{min} = 10^{-2}$ as the contrast sensitivity, an oil immersion objective ($n_{ob} = 1.5$) and the typical values for isotonic RBCs, $\Delta n = 0.06$, and $\bar{\kappa} = 0.7 \mu\text{m}^{-1} = 0.7 \times 10^{-3} \text{nm}^{-1}$, the minimum axial distance is approximately 180 nm, sufficient to resolve the axial separation of the RBCs surface-membranes, for all solution osmolalities studied. In Fig.3 a total 3D image of a RBC in a hypertonic solution is presented, showing that we are able to resolve the distance between the two membrane surfaces at the cell center, which is 300 nm and therefore confirms the estimates above (see movie *S4* in supplementary materials¹⁴).

In order to obtain $H(\vec{\rho})$ we need the value for Δn , which is basically defined by the RBC hemoglobin concentration. A good assessment of the red cell refractive index (n_{rbc}) can be obtained by measuring the distance between the minimum contrast plane to the glass coverslip plane, which is $|h_{2,m}|$ in the RBC rim position. The layout of the refractive index experiment is seen in Fig.1a, where polystyrene beads of diameter $d = 0.198 \mu\text{m}$ are deposited on the glass coverslip, such that the location of the glass slide is determined from a z-scan throughout the bead defocused images. The minimum

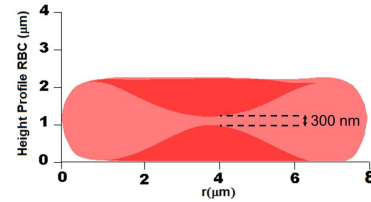


FIG. 3. Total 3D image of a RBC in a hypertonic solution (400 mOsm/Kg). The surface-membranes are clearly imaged, indicating that the axial resolution in this case is better than 300nm (Multimedia view).

bead contrast occurs when the objective focal plane coincides with its diameter, from where we move the objective until the RBC minimum contrast plane (largest diameter plane). To be more quantitative, one can select images around the bead and around the RBC as the objective focal plane is scanned. The recorded images must contain the bead and the RBC completely, as shown in Fig.1(b-d). Since there is no light absorption, the spatial average intensity of the complete

image is equal the background intensity, $\langle I \rangle_{\bar{\rho}} = I_0 = (1/N_p) \sum_i I_i$, where N_p is the total number of pixels of the image and I_i is the intensity of each pixel. In order to define the minimum contrast position we calculate the standard deviation of the spatially averaged intensity I for each frame and divide it by I_0 , which corresponds to $\sqrt{\langle I^2 \rangle - \langle I \rangle^2} / \langle I \rangle = \sqrt{\langle \Delta C^2 \rangle_{\bar{\rho}}}$, with $\langle I^2 \rangle = (1/N_p) \sum_i (I_i)^2$. In Fig.1e, the behaviour of $\sqrt{\langle \Delta C^2 \rangle_{\bar{\rho}}}$ as a function of z_f is shown, from which the minimum values of $\sqrt{\langle \Delta C^2 \rangle_{\bar{\rho}}}$ for a RBC ($z_f = 0$) and of the polystyrene bead ($z_f = z_{bead}$) are clearly determined. Hence, $|h_{2m}| = |z_{bead}| + |r_{bead}| = |z_{bead}| + 0.099\mu m$. The obtained values for the RBC refractive ($\lambda = 0.610\mu m$) are shown in Table 1, in agreement with results obtained using different techniques^{5,22}. As expected, due to water entrance into the cell, for the hypotonic solution n_{rbc} is lower than in the other cases.

In conclusion, in this paper we present a novel methodology to obtain total 3D imaging of phase objects using a defocused bright-field optical microscope. We apply the method to RBCs subject to different solution osmolalities and determine the cell shapes and surface-membranes deformation due to adhesion to the glass-substrate. Strikingly, our results show that the Defocusing Microscopy axial resolution for RBCs can be smaller than 300nm, allowing a clear imaging of both surface-membranes. In addition, we obtain the cell average refractive index, surface area, volume and sphericity index over a group of 25 red blood cells under different osmotic conditions, showing that DM technique can be used for monitoring certain pathologies. Since DM does not require the use of any extra optical element, the technique could be easily adopted by non-specialists.

¹F. Zernike, Physica **9**, 686 (1942).

- ²G. Nomarski, J. Phys. Radium **16**, 9 (1955).
³D. Paganin and K. A. Nugent, Phys. Rev. Lett. **80**, 2586 (1998).
⁴E. D. Barone-Nugent, A. Barty, K. A. Nugent, J. Micros. **206**, 194 (2002).
⁵B. Rappaz et al., Cytometry **73A**, 895 (2008).
⁶G. Popescu et al., Blood Cells Mol. Dis. **41**, 10 (2008).
⁷V. L. Kononenko, Wiley-VCH Verlag GmbH Co. KGaA. 155 (2011).
⁸G. Glionna et al., Appl. Phys. Lett. **15 94**, 193701 (2009).
⁹L. Siman et al., submitted to publication (2014).
¹⁰T. Kim et al., Nature Photonics, Advance Online Publication, 19 January (2014).
¹¹M. R. Teague, J. Opt. Soc. Am. **73**, 1434 (1983).
¹²M. Born and E. Wolf, "Principles of Optics", Cambridge University Press, New York (1999).
¹³J. W. Goodman, "Introduction to Fourier Optics," McGraw-Hill Co., Inc.(2002).
¹⁴See supplementary material at () for thickness profile results, movies of red cells 3D imaging, as well as information on the experimental set up, materials and procedures.
¹⁵L. G. Mesquita, U. Agero, and O. N. Mesquita, Appl. Phys. Lett. **88**, 133901 (2006).
¹⁶U. Agero et al., Phys. Rev. E **67**, 051904 (2003).
¹⁷J. C. Neto et al., Exp. Cell Res. **303 (2)**, 207 (2005).
¹⁸J. C. Neto et al., Biophys. J. **91**, 1108 (2006).
¹⁹Y. Park et al., Phys. Rev. E **83**, 1051925 (2011).
²⁰B. Rappaz et al. Blood Cell, Mol. Dis. **42**, 1 (2009).
²¹E. Evans and Y. C. Fung, Microvascular Research **4**, 335 (1972).
²²A. L. Yusipovich et al., J. Appl. Phys. **105**, 102037 (2009).
²³P. B. Canham and A. C. Burton, Circulation Research **22**, 405 (1968).
²⁴P. B. Canham, J. Theor. Biol. **26**, 61 (1970).

Acknowledgements

We would like to acknowledge the financial support from the Brazilian Agencies CNPq, FAPEMIG, PRONEX-FACEPE, Instituto Nacional de Fluidos Complexos e Aplicações (INFCx) and FAPEAM. The authors also thank Michael O'Carroll for useful discussions.

Supporting Information:

Total 3D imaging of phase objects using defocusing microscopy: application to red blood cells

P. M. S. Roma¹, L. Siman¹, F. T. Amaral², U. Agero¹ and O. N. Mesquita^{1, a)}

¹Departamento de Física, ²Programa de Pós Graduação em Engenharia Elétrica, Universidade Federal de Minas Gerais, Caixa Postal 702, CEP 31270-901, Belo Horizonte, MG, Brazil.^{a)}

A. Defocusing Microscopy Instrumentation

Experiments were conducted on inverted microscopes operating in bright field (Nikon TE300 and Nikon Eclipse TI-E) with oil immersion objectives (Nikon Plan APO DIC H, 100X, 1.4 NA and Nikon Plan APO DIC H, 100X, 1.49 NA; Nikon, Melville, NY). Images of RBCs were captured with a CMOS camera (CMOS 642M) at a typical frame rate of 300fps. The defocusing distance was controlled by a piezoelectric nanoposition stage (P563-3CD, Physik Instrumente (PI) GmbH Co, Karlsruhe, Germany) coupled to the microscope stage. Perfect Focus System (Nikon) was used to stabilize the focus. A red filter ($\lambda = 0.61\mu\text{m}$) was added into the microscopes optical paths in order to avoid absorbing effects by RBCs.

B. Cell Sample Preparation

Briefly, approximately $0.5\mu\text{L}$ of fresh blood is collected from healthy laboratory personnel, and suspended in a 1.5ml solution of phosphate-buffered saline (PBS) (pH 7.4, NaCl 150 mM) with 1.0mg/mL of bovine serum albumin (Sigma Aldrich, St. Louis, MO)¹. This solution has a refractive index of $n_{\text{solution}} = 1.333 \pm 0.001$ and represents our isotonic solution (NaCl 0.9% - 300 mOsm/kg). We adjusted the NaCl concentrations to 0.6% and 1.2% to obtain the desired osmolality corresponding to hypotonic (200 mOsm/kg) and hypertonic (400 mOsm/kg) solutions, respectively. The osmolality of each solution was measured with a freezing-point depression osmometer (Advanced Model 3250 Single-Sample Osmometer). For each experiment, a $250\mu\text{L}$ volume of the RBCs suspension was transferred to a microscope cover glass chamber and covered with a coverslip to avoid water evaporation. For refractive index measurements, the same volume of the RBC suspension was transferred to a pre-treated cover glass with polystyrene beads (Polysciences, Inc, Warrington, PA, USA) of $0.198\mu\text{m}$. Samples were made immediately before experiments and left still on the microscope stage for approximately 15 minutes to allow cell precipitation and adhesion. On average, each experiment lasts for two hours. All experiments were conducted at room temperature ($\sim 27^\circ\text{C}$).

C. Thickness Profile

The mean thickness results for 25 cells in hypotonic, isotonic, and hypertonic solutions are shown in Fig. 1. In Fig. 1(a - c), a red cell thickness map immersed in each situation is presented and in (d - f) the respective 3D thickness images are shown. The 3D thickness image is obtained using ImageJ Interactive 3D Surface Plot plugin software package (Rasband WS. ImageJ, U.S. National Institutes of Health, Bethesda, Maryland, USA, imagej.nih.gov/ij/, 19972012)² over the thickness map. The mean thickness profile and cell radius obtained is in agreement with previous findings³⁻⁵. In Fig.1(g - i) the average radial profile over each set of 25 RBCs are presented, indicating that the medium osmolality influences the cell shape. In the hypotonic medium (Fig.1g, the RBCs are swollen due to water influx, losing its discoid shape exhibited in isotonic solution (Fig. 1h). In the hypertonic case (Fig.1i), the RBCs suffers water efflux, such that the dimpled region in the center becomes more pronounced.

D. Image processing and numerical procedures

Images captured with a CMOS camera are later processed, because even under uniform illumination the background gray level of each pixel is not uniform. We used a correction procedure as established on the ImageJ Information and Documentation Portal website. This procedure consists of filming the area of interest without RBCs, with uniform illumination, and measure the gray level of each pixel. Later the gray level of each pixel of the images with the RBCs are divided by the background gray level, measured previously. Therefore, any pixel inhomogeneity is eliminated. All captured images were analyzed using NIH-ImageJ software package, Java plugins and algorithms in Matlab (The Mathworks Inc., Natick, MA) developed in our group to perform the complete 3D reconstruction. The model fitting was implemented using Matlab's `lsqcurvefit` function, which is based on least squares method. The asymmetry parameter was adjusted in order to fit the analytical expression presented on equation (8) to the experimental data. The least squares method requires a starting value to the fitting parameter. We set 0 as the starting value to δ for the tests after being observed that the convergence of the algorithm was satisfactory for this initial guess. How-

^{a)}E-mail me at: mesquita@fisica.ufmg.br

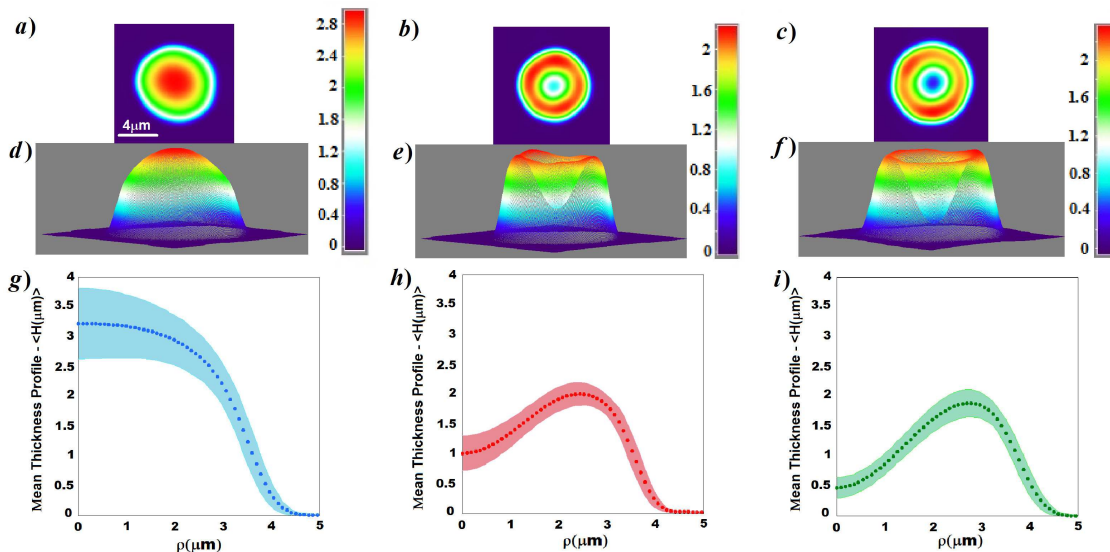


FIG. 1. Thickness profile map of red blood cells immersed in a (a) hypotonic (200 mOsm/kg), (b) isotonic (300 mOsm/kg), and (c) hypertonic (400 mOsm/kg) solutions, and its respective 3D thickness reconstruction (d - f). (g - h) Mean thickness radial profile for the 25 analyzed cells in each solution. The shaded areas represent the standard deviations.

ever, we tested different initial guesses of the parameter δ , which also yielded optimal solutions and returned the same result for $\delta(\bar{\rho})$, showing that the fitting method is robust and appropriate to be applied to the problem of 3D imaging of phase objects. Then for all subsequent fittings we started from $\delta(\bar{\rho}) = 0$. The stop criteria used on the optimization routine was the sum at squared error less or equal than 0.1% of the experimental data variance. In average, after 10 iterations the algorithm converged.

E. Video of RBC Total 3D Imaging

Movie S1. The movie file *Hypotonic.mov* illustrates the total 3D Imaging of a RBC immersed in a hypotonic solution (200 mOsm/Kg). The upper surface-membrane is inflated due to water influx and presents a nearly spherical profile, while the lower surface-membrane becomes flat and almost completely attached to the glass-substrate.

Movie S2. The movie file *Isotonic.mov* illustrates the total 3D Imaging of a RBC immersed in an isotonic solution (300 mOsm/Kg). The cell has a biconcave shape

and the lower surface-membrane has a flatter profile than the upper one, due to adhesion to the glass-substrate.

Movie S3. The movie file *Hypertonic1.mov* illustrates the total 3D Imaging of a RBC immersed in a hypertonic solution (400 mOsm/Kg). Due to water efflux, the center separation distance between the lower and the upper surface-membranes is decreased and a more pronounced dimple in the center is seen.

Movie S4. The movie file *Hypertonic2.mov* illustrates the total 3D Imaging of a RBC immersed in a hypertonic solution (400 mOsm/Kg), with a distance between the two surface-membranes at the cell center of 300nm. As can be seen, we are able to obtain a more complete assessment of the shapes and deformations of the two surface-membranes for different angles of view.

All movies are rotations of a static RBC which was first rotated in z and then in x axis for 360°.

¹L. G. Mesquita, U. Agero, and O. N. Mesquita, Appl. Phys. Lett. **88**, 133901 (2006).

²C. A. Schneider et al., Nature Methods **9** 671 (2012).

³G. Popescu et al., Blood Cell, Mol. Dis., **41**, 10 (2008).

⁴Y. Park et al., Phys. Rev. E **83**, 051925 (2011).

⁵B. Rappaz et al., Blood Cell, Mol. Dis., **42** 1 (2009).